Theoretical Model for Electrophilic Oxygen Atom Insertion into Hydrocarbons

Robert D. Bach,*,‡ José L. Andrés,†,‡ Ming-Der Su,‡ and Joseph J. W. McDouall§

Contribution from the Department of Chemistry, Wayne State University, Detroit, Michigan 48202, and Department of Chemistry, University of Manchester, Manchester M13 9PL, U.K.

Received September 19, 1991

Abstract: A theoretical model suggesting the mechanistic pathway for the oxidation of saturated alkanes to their corresponding alcohols and ketones is described. Water oxide (H_2O–O) is employed as a model singlet oxygen atom donor. Molecular orbital calculations with the 6-31G* basis set at the MP2, QCISD, QCISD(T), CASSCF, and MRCI levels of theory suggest that oxygen insertion by water oxide occurs by the interaction of an electrophilic oxygen atom with a doubly occupied hydrocarbon fragment orbital. The electrophilic oxygen approaches the hydrocarbon along the axis of the atomic carbon p orbital comprising a π_{CH_2} or π_{CHCH_3} fragment orbital to form a carbon–oxygen σ bond. A concerted hydrogen migration to an adjacent oxygen lone pair of electrons affords the alcohol insertion product in a stereoselective fashion with predictable stereochemistry. Subsequent oxidation of the alcohol to a ketone (or aldehyde) occurs in a similar fashion and has a lower activation barrier. The calculated (MP4/6-31G*//MP2/6-31G*) activation barriers for oxygen atom insertion into the C–H bonds of methane, ethane, propane, butane, isobutane, and methanol are 10.7, 8.2, 3.9, 4.8, 4.5, and 3.3 kcal/mol, respectively. We use *ab initio* molecular orbital calculations[5] in support of a frontier MO theory that provides a unique rationale for both the stereospecificity and the stereoselectivity of insertion of electrophilic oxygen and related elcectrophiles into the carbon–hydrogen bond.

Introduction

One of the remaining frontiers in organic chemistry is the direct functionalization of saturated hydrocarbons. Considerable progress has been made in understanding the chemical requirements for transition-metal "activation" of carbon–hydrogen bonds.[1] The catalytic cycle that oxidizes a hydrocarbon RH to an alcohol ROH employing cytochrome P-450 is also a well-established reaction.[2] More recently, the remarkable chemical reactivity of dimethyldioxirane and methyl(trifluoromethyl)-dioxirane[3a,b] has been demonstrated by its ability to insert oxygen atoms into hydrocarbons by what appears to be a highly stereoselective concerted process.[3c–e] Although these reactions have many features in common, a unifying mechanism for electrophilic insertion into σ bonds has not yet appeared. In this report we describe a frontier molecular orbital (FMO) model, based upon a set of fragment hydrocarbon molecular orbitals, that allows one to predict the approximate axis of attack of an electrophilic reagent on a carbon–hydrogen σ bond.

Mechanistic considerations of hydrocarbon insertion reactions typically focus upon initial attack of the electrophilic species at approximately 90° to the σ C–H bond, as shown in **1**. In this orientation, the interacting orbitals approach each other at right angles with typically poor overlap and mixing of the electron density of the σ bond with the attacking electrophile and with the relatively high-energy C–H σ* orbital.[1a] In a canonical molecular

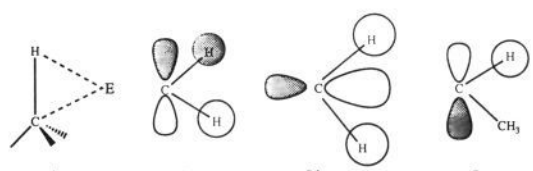

1 **2a** **2b** **2c**

orbital description of a hydrocarbon, there are no isolated MOs that describe a particular C–H σ bond. For example, in methane there is a lower lying $^2A_1$ orbital and three degenerate T_2 orbitals.[4a] In a tetrahedral array, both hydrogens (or carbons) directly bound to the sp^3 carbon occupy a common plane, and they are related by symmetry and may comprise an orbital with π symmetry (π_{CH_2}) as in **2a** or a σ_{CH_2} orbital as in **2b**.[4a] Therefore, interaction of an electrophile with methane will involve both hydrogens in the CH_2 fragment orbital. The migrating hydrogen will necessarily be perturbed more by the insertion process than the other hydrogen in the π_{CH_2} fragment. Replacement of one of the hydrogens in a π_{CH_2} fragment orbital by a methyl group gives rise to the π_{CHCH_3} orbital (**2c**).

In this idealized model we define the electrophilic reagent E as having an electron-deficient orbital to interact with the doubly occupied hydrocarbon fragment orbital and one or more pairs of electrons that may serve as the migration terminus for a 1,2-hydrogen shift (eq 1). The rationale for using fragment orbitals 2a–2c to describe the orientation of attack is that the σ/π nomenclature is the natural one to use when discussing the problem in a set of canonical Hartree–Fock orbitals. The localized description of the CH bond is equally valid but very much harder to reconcile with the geometries obtained for the transition states.

† Departament de Química, Universitat Autonoma de Barcelona, 08193 Bellaterra, Catalonia, Spain.
‡ Wayne State University.
§ University of Manchester.

(1) (a) *Activation and Functionalization of Alkanes*; Hill, C. L., Ed.; John Wiley and Sons: New York, 1989. (b) Crabtree, R. H. *Chem. Rev.* **1985**, *85*, 245. (c) Janowicz, A. H.; Berman, R. G. *J. Am. Chem. Soc.* **1983**, *105*, 3929. Stoutland, P. O.; Bergman, R. G. *Ibid.* **1988**, *110*, 5732. (d) Hoyano, J. K.; McMaster, A. D.; Graham, W. A. E. *J. Am. Chem. Soc.* **1983**, *105*, 7190.

(2) *Cytochrome P-450*; Montellano, P. R., Ed.; Plenum Press: New York, 1986. Ingold, K. U. *Aldrichim. Acta* **1989**, *22*, 69.

(3) (a) Murray, R. W. *Chem. Rev.* **1989**, *89*, 1187. (b) Adam, W.; Curci, R.; Edwards, J. O. *Acc. Chem. Res.* **1989**, *22*, 205. (c) Murray, R. W.; Jeyareman, R.; Mohan, L. *J. Am. Chem. Soc.* **1986**, *108*, 2476. (d) Mello, R.; Rlorention, M.; Fusco, C.; Curci, R. *J. Am. Chem. Soc.* **1989**, *111*, 6749. (e) Adam, W.; Asensio, G.; Curci, R.; Gonzalez-Nunez, M. E.; Mello, R. *J. Org. Chem.* **1992**, *57*, 953. (f) Mello, R.; Cassidei, L.; Fiorentino, M.; Fusco, C.; Hümmer, W.; Jäger, V.; Curci, R. *J. Am. Chem. Soc.* **1991**, *113*, 2205.

(4) (a) For a discussion, see: Jorgensen, W. L.; Salem, L. *The Organic Chemist's Book of Orbitals*; Academic Press: New York, 1973. (b) Meredith, C.; Hamilton, T. P.; Schaefer, H. F., III *J. Phys. Chem.* **1992**, *96*, 9250.

0002-7863/93/1515-5768$04.00/0

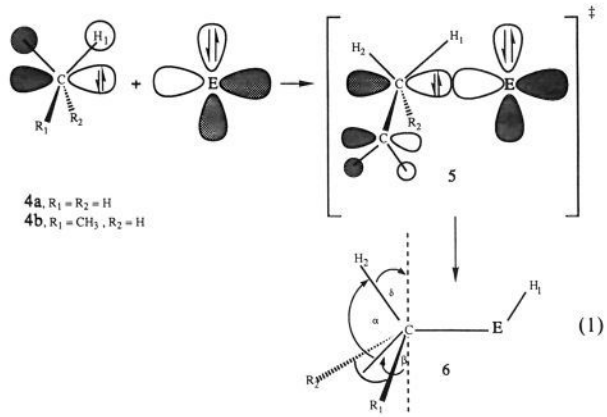

By using the canonical MOs, it is possible to show that the transition states arise from a simple juxtaposition of electron-donating and -accepting orbitals. The π_{CH_2} fragment orbital is easily visualized in a "modeling" sense, and the C–E axis of attack of the approaching E^+ is more readily defined (**3a**, Figure 1). Thus, a filled hydrocarbon π_{CH_2} fragment in **4** overlaps with an empty orbital on E to arrive at transition state **5**. The H_1–C–E bond angles in **5** will depend upon the C–E bond distance and the number of alkyl substituents on the "nucleophilic" carbon atom involved. In this orientation the migrating hydrogen (H_1) is ideally poised for a concomitant 1,2-hydrogen shift to the adjacent electrophilic atom (oxygen) in the transition state. In the case of water oxide (H_2O–O), the electrophilic empty orbital is the σ^* O–O orbital and the neutral leaving group is water.

Although we would have preferred to use dioxirane as the oxygen donor, computational difficulties with this highly strained molecule[5] prompted us to use water oxide in this initial study. We suggest that water oxide is a suitable oxygen-donor model for dioxirane. Our calculations predict that both oxygen donors react almost exclusively by a closed-shell pathway and that they exhibit similar reactivities toward alkene epoxidation and the oxidation of ammonia.[5] The reactive form of hydrogen peroxide, when it is serving as a oxygen atom donor in the gas phase, is calculated to be water oxide[5a] (H_2O^+–O^-). Since insertion of a singlet oxygen atom (^1O) into a hydrocarbon typically occurs without a barrier, the opportunity to examine relative activation barriers for different approaches of E is lost. We have found that an activation barrier is predicted with oxygen atom donation from water oxide because of the O–O bond rupture, and consequently this parent oxonium ylide serves as an ideal model oxygen atom donor in theoretical studies. Our results suggest that water oxide is a high-energy intermediate since it is calculated to be 49.7 kcal/mol above ground-state hydrogen peroxide[5b] and the barrier for its 1,2-hydrogen shift to revert back to H_2O_2 is only 3.2 kcal/mol.[4b] Since the barrier for a 1,2-hydrogen shift in concert with oxygen atom transfer from hydrogen peroxide is prohibitively high, oxygen donation from hydrogen peroxide in solution requires either a proton relay mechanism or extensive solvation.[5a,b] Although the "electrophilic" oxygen of water oxide is negative in its ground state, in the transition state it is more like an electrophilic singlet oxygen atom. An ideal oxygen-transfer reagent is one that has an essentially naked oxenoid oxygen possessing a complete octet of electrons that can afford an electrophilic oxygen atom with only six electrons in its outer shell upon the departure of a neutral leaving group.

(5) (a) Bach, R. D.; McDouall, J. W.; Owensby, A. L.; Schlegel, H. B. *J. Am. Chem. Soc.* **1990**, *112*, 7065; *112*, 7064. (b) Bach, R. D.; McDouall, J. W.; Owensby, A. L.; Schlegel, H. B. *J. Am. Chem. Soc.* **1990**, *112*, 6001. (c) Bach, R. D.; Andrés, J. L.; Owensby, A. L.; Schlegel, H. B. *J. Am. Chem. Soc.* **1992**, *114*, 7207. (d) Bach, R. D.; Owensby, A. L.; Gonzalez, C.; Schlegel, H. B. *J. Am. Chem. Soc.* **1991**, *113*, 2338.

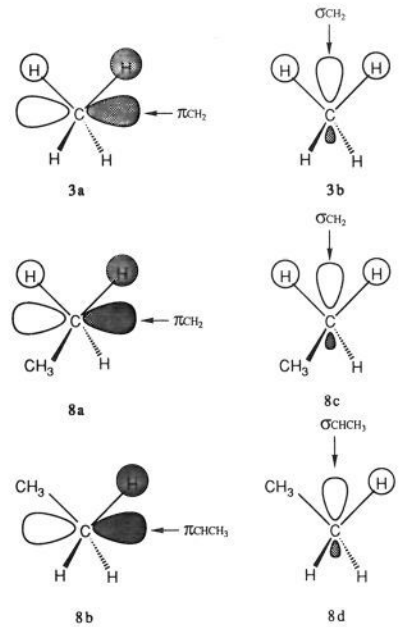

Figure 1. Orientation of electrophilic attack on methane and ethane.

Method of Calculation

Molecular orbital calculations were carried out using the GAUSSIAN 92 program system[6a] utilizing gradient geometry optimization.[6b] The reactants and transition structures were fully optimized at the MP2/6-31G* level. Relevant energies and barrier heights were computed with the 6-31G* basis set using fourth-order Møller–Plesset perturbation theory (frozen core, MP4SDTQ/6-31G*//MP2/6-31G*). Unless noted otherwise, all structures were established to be either minima or first-order transition states that exhibited a single imaginary frequency at the MP2/6-31G* level using either GAUSSIAN 92[6a] or CADPAC.[6c] Complete active space SCF calculations (CASSCF) were performed using the GAMESS package.[6d] Multireference CI calculations were performed on the basis of CASSCF configurations using the MR-CI code of Saunders and Van Lenthe as implemented in GAMESS (Daresbury version).[6d]

Results and Discussion

(a) Oxygen Insertion into Methane. There are two unique approaches of an electrophilic species to methane; the empty orbital of the electrophile may either interact with a filled MO with π symmetry (π_{CH_2}), as depicted in **3a**, or approach in a σ_{CH_2} fashion, as shown in **3b** (Figure 1). In the simplest example, we calculate the lowest energy path ($\Delta E^\ddagger = 10.7$ kcal/mol) for oxygen insertion into methane (**TS-1**) to involve interaction of a filled σ_{CH_2} fragment with the oxenoid oxygen of water oxide (Figure 2).[7] The barrier for oxygen insertion into the π_{CH_2} fragment orbital of methane (**9**) was only slightly higher in energy (11.2 kcal/mol, second-order saddle point). Release of the geometry constraint for a π_{CH_2} approach (**9**) resulted in convergence to **TS-1** that was shown to be a first-order saddle point by an analytical frequency calculation at the MP2/6-31G* level.[7] A fourth-order Møller–Plesset electron correlation correction has

(6) (a) Frisch, M. J.; Trucks, G. W.; Head-Gordon, M.; Gill, P. M. W.; Wong, M. W.; Foresman, J. B.; Johnson, B. G.; Schlegel, H. B.; Robb, M. A.; Replogle, E. S.; Gomperts, R.; Andres, J. L.; Raghavachari, K.; Binkley, J. S.; Gonzalez, C.; Martin, R. L.; Fox, D. J.; Degrees, D. J.; Baker, J.; Stewart, J. J. P.; Pople, J. A. *GAUSSIAN 92*; Gaussian, Inc.: Pittsburgh, PA, 1992. (b) Schlegel, H. B. *J. Comput. Chem.* **1982**, *3*, 214. (c) Amos, R. D.; Rice, J. E. CADPAC: Cambridge Analytical Derivatives Package, Issue 4, Cambridge, 1988. (d) Guest, M. F. *GAMESS*; Daresbury Laboratory: U.K.

(7) Optimization at MP2/6-31G* is essential for obtaining adequate geometries of the O–O bond, and fourth-order Møller–Plesset electron correlation correction is required for energetics.[5] All energies are reported at MP4SDTQ/6-31G*//MP2/6-31G* unless specified otherwise. Analytical frequency calculations at MP2/6-31G* using CADPAC[6c] established the validity of **TS-1**, **TS-2**, and **TS-3**. Frequency calculations (MP2/6-31G*) on the remaining structures utilized GAUSSIAN 92.

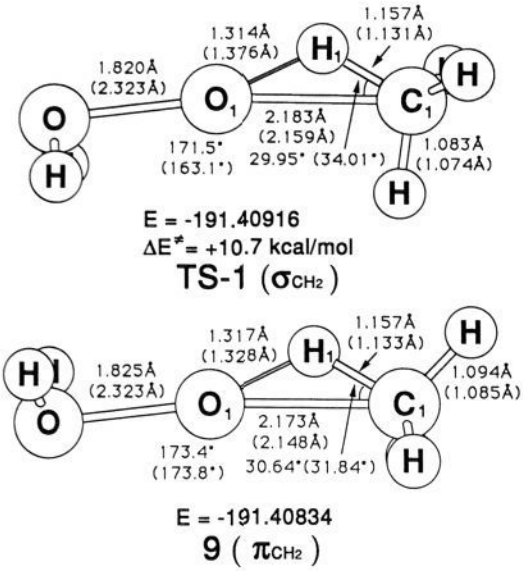

Figure 2. Transition structure (TS-1) and second-order saddle point **9** on the potential energy surface for oxygen and atom transfer from water oxide to methane. Geometries are MP2/6-31G* (HF/6-31G* values are in parentheses). Distances are in angstroms and angles in degrees. Activation energies are MP4SDTQ/6-31G*//MP2/6-31G*, au.

a fairly significant lowering effect (2.8 kcal/mol) upon the magnitude of the activation barrier (Table I).

The transition state for the highly exothermic (–100.4 kcal/mol) oxidation of methane comes early along the reaction coordinate, as evidenced by the minimal geometric distortion of the CH_4 hydrocarbon portion of **TS-1**, which is only 2.3 kcal/mol higher in energy (HF/6-31G*) in the transition state than in ground-state methane. The O–O bond (1.517 Å) in water oxide is elongated by 0.67 Å in the transition state. Interestingly, the O–O bond distance in the **TS** for oxygen transfer from H_2O–O to ammonia (1.68 Å),[5a] a better nucleophile than methane, is 0.14 Å shorter than that in **TS-1**. The calculated Mulliken charges on O_1 and O_2 in water oxide are –0.400 and –0.600, while those in **TS-1** are –0.323 and –0.780, reflecting the lower electron density on the electrophilic oxygen (O_1) as the water molecule departs.

We use the π_{CH_2} approach in the second-order saddle point **9** (Figure 2) to illustrate the overall molecular motion required for oxygen insertion into methane, since the preferred orientation for approach of the electrophile is π_{CH_2} in nature when alkyl or oxygen substituents are present on the carbon. As anticipated, the oxygen atom approached the filled π_{CH_2} fragment of methane along the axis of the atomic 2p orbital as suggested by eq 1. Although the electrophilic E approaches the carbon along its p axis in the transition state, after insertion and concomitant hydrogen (H_1) migration the electrophilic atom E must ultimately lie approximately on the C–H_1 bond axis of the initial hydrocarbon. This requires molecular reorganization through angle θ, as shown in **7**. The angle θ in **7** between the migrating hydrogen and the p orbital in methane (**4a**) is 35.3 in the ground state (HF/6-31G*) and 30.6 in the second-order saddle point **9** (Figure 2).

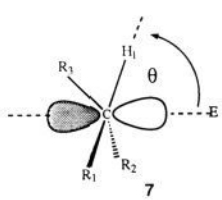

7

After the barrier is crossed, the methyl group must tilt, as indicated in **6** (eq 1), in order that the final orientation of the C–O bond in the methanol product (**6**, E = O) be approximately that of the C–H bond in the starting material methane as depicted in **7**. Hydrogen H_2 (eq 1) moves through an angle $\Delta\delta$ = 38.5° (from 54.7° in methane to a final angle of 16.3° in methanol), while the R_1CR_2 plane rotates clockwise by β = 22.3°. In the transition state the H_1–C–H_2 bond angle contracts to 101.5°, while that angle in the orthogonal CH_2 fragment expands to 111.8°. Optimization of **TS-1** at the QCISD/6-31G* level of theory afforded a geometry where the O–O (1.92 Å) and the C–O (2.20 Å) bond distances are in good agreement with the MP2/6-31G* geometry. The O–C–H_1 angle of 31.9° is also consistent with those values given in Figure 2.

(b) Oxygen Insertion into Ethane. There are four different orientations for electrophilic insertion into a σ_{CH} bond of ethane. There are two equivalent approaches of the electrophile to both sides of the π_{CH_2} orbital in ethane as depicted in **8a**, and there is also a π_{CHCH_3} approach, as indicated in **8b**. The two additional potential transition structures involve interaction of E with σ_{CH_2} (**8c**) and σ_{CHCH_3} (**8d**) fragment orbitals. Steric considerations suggest that an electrophile will not approach in a σ_{CHCH_3} (**8d**) fashion when the methyl group of the fragment orbital is replaced by a larger alkyl group. We have examined the π_{CH_2} (**8a**), π_{CHCH_3} (**8b**), σ_{CH_2} (**8c**), and σ_{CHCH_3} (**8d**) approaches of E to ethane. In **TS-2** (Figure 3), insertion into the π_{CH_2} fragment occurs with a methyl substituent ($R_1 = CH_3$ in **4b**) at right angles to the plane of the π_{CH_2} orbital ($\Delta E^{\ddagger}$ = 8.2 kcal/mol). Electrophilic insertion into the C–H bond in this first-order saddle point is influenced electronically by the filled adjacent methyl group fragment orbitals, as depicted in **5**. The filled atomic 2p orbital of the π_{CH_2} fragment approaches the O–O σ^* orbital from the backside in an S_N2 fashion, ultimately resulting in the displacement of a water molecule.

In **10** (Figure 3), a methyl group lies in the plane of the migrating hydrogen (H_1) and the electrophile attacks a π_{CHCH_3} fragment orbital (**2c**). The latter C_s structure is a second-order saddle point that lies 1.1 kcal/mol above the energy of **TS-2** (Table I). The σ_{CHCH_3} approach in **11** is also a second-order saddle point that lies 0.5 kcal/mol above the energy of **TS-2**. The transition structure and reaction trajectory for oxygen insertion closely resemble those for π_{CH_2} insertion into methane (**9**), where the pertinent angle θ (see **7**) in methane is 30.6° and that in ethane is 28.8°. The barrier for **TS-2** is 3.0 kcal/mol lower than that for insertion into methane, reflecting the potential stabilizing influence of the adjacent parallel π_{CH_2} fragment of the methyl group, as shown in **5**. However, the charges on carbon and H_1 in ethane are –0.47 and 0.16, while those in **TS-2** are –0.48 and 0.19, respectively. In general, the calculated Mulliken charge on carbon actually increases slightly (0.01e) on going from the ground to the transition state. This is a reflection of the repulsive interaction between the electron density at carbon and the lone pairs of electrons on the transferring oxygen. The electrophilic nature of water oxide may be attributed to a facile lowering of the energy of the σ^* O–O orbital attending O–O bond elongation. The negative charges on C_1 in the TS for ethane, propane, and isobutane insertion (–0.48, –0.31, and –0.16) show a steady decrease with increasing alkyl substitution. The positive charge on H_1 shows an increase of ~0.1 upon going from the ground to the transition state for oxidation of propane and isobutane (see **TS-4** and **TS-6**).

Although oxygen insertion into ethane via the σ_{CH_2} approach (**12**) involves an adjacent methyl group that can potentially stabilize the developing positive charge attending hydrogen migration, **12** is also a second-order saddle point. When all geometric constraints are released, this geometry converges to **TS-2** (a first-order saddle point at MP2/6-31G*)[7] as the only real transition structure that we have identified on this potential energy surface. We attribute this to the greater efficiency of overlap of an adjacent π_{CH_2} fragment orbital of the methyl group when it is more nearly parallel to the principal C–E bond axis for the insertion reaction, as depicted in **5**. Plots of the molecular

Table I. Potential Energy Barriers (kcal/mol) for Oxygen Insertion Into Carbon–Hydrogen Bonds (6-31G*)

substrate	compd	orientation	HF	MP4//HF	MP2	MP4//MP2[a]	PMP4/MP2[b]
methane							
methane	**9**	π_{CH_2}[c]	14.4	14.8	14.0	11.2	
	TS-1	σ_{CH_2}[d]	14.5	14.2	13.5	10.7	13.9
ethane							
	TS-2	π_{CH_2}[d]	12.4		10.8	8.2	11.4
	10	π_{CHCH_3}[c]	13.2	13.0	11.9	9.3	
	11	σ_{CH_2}[e]	12.9		11.3	8.7	
methanol							
	TS-3	π_{CH_2}[d]	9.3	6.7	5.8	3.3	5.9
	12	π_{CHCH_3}[c]	14.6	15.3	12.3	9.6	
	13	σ_{CH_2}[e]	12.5	9.3	9.3	6.4	

[a] The MP4SDTQ/6-31G*//MP2/6-31G* energies (au) for methane, ethane, methanol, and water oxide are −40.354 58, −79.532 81, −115.378 85, and −151.071 56, respectively. [b] Barriers computed with reoptimized molecular orbitals at the MP2/6-31G* geometries. [c] These geometries are second-order saddle points at MP2/6-31G*. [d] These geometries are first-order saddle points at MP2/6-31G*. [e] These geometries are restricted to be in this orientation.

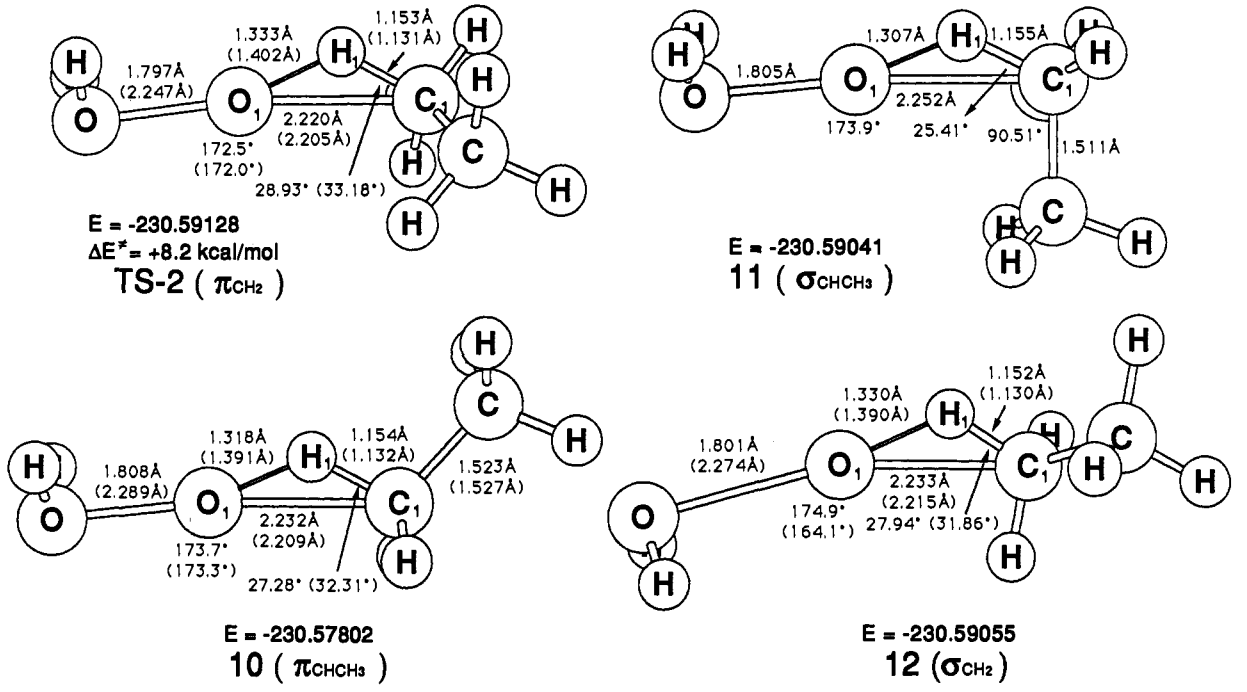

Figure 3. Transition structure **TS-2** and second-order saddle points **10**, **11**, and **12** on the potential energy surface for oxygen atom transfer from water oxide to ethane. Geometries are MP2/6-31G* (HF/6-31G* values are in parentheses). Distances are in angstroms and angles in degrees. Activation energies are MP4SDTQ/6-31G*//MP2/6-31G*, au.

orbitals of these transition structures are consistent with the idealized pictures shown. In all three orientations, the electrophile approaches the fragment orbital at its point of maximum electron density, the carbon atomic 2p orbital.

Oxygen-transfer reactions have been shown to possess unstable Hartree–Fock solutions to the wave function in many cases.[5] To check the validity of our calculations, stability analyses were performed for these transition structures. All wave functions showed a RHF → UHF instability, indicating that a lower energy UHF solution existed. UHF wave functions were obtained by applying a symmetry-breaking transformation to the RHF orbitals involving the mixing of HOMO and LUMO. After internal stability of the UHF solutions was checked, the activation barriers for **TS-1**, **TS-2**, and **TS-3** were recalculated at the MP4 level, including spin-projection (PMP4) according to Schlegel's scheme.[8] In all cases this procedure yielded an increase in the activation energy, the largest change being +4.5 kcal/mol for **TS-2** (Table I).

In related oxygen-transfer reactions involving water oxide[5a–c] and peroxyacids,[5d] we have established the importance of dynamic electron correlation to adequately treat both the geometry and the energetics of transformations involving the O–O bond. We therefore optimized the geometry for the transition state for the oxidation of ethane for water oxide at the QCISD/6-31G* level. The activation barrier for **TS-2** was calculated to be 14.4 kcal/mol. However, with the contribution from the triples (QCISD-(T)/6-31G*//QCISD/6-31G*), the activation energy was reduced to 7.4 kcal/mol, in good agreement with the MP4SDTQ barrier of 8.2 kcal/mol. The C_1–O_1 bond distance (Figure 4) does not differ significantly from that found at the MP2 level (Figure 3), but the O–O bond is more elongated (0.09 Å). With that exception the two methods are in good agreement. While reliable geometries are obtained from higher-order methods such as QCISD, the contributions of the dynamic and static correlations effects are difficult to separate. We therefore chose to further pursue this oxygen insertion process using complete active space SCF (CASSCF)[9] theory to elucidate the role of the structure-dependent correlation in **TS-2**.

(8) (a) Schlegel, H. B. *J. Phys. Chem.* **1988**, *92*, 3075. (b) Schlegel, H. B. *J. Chem. Phys.* **1986**, *84*, 4530.

(9) Eade, R. H. A.; Robb, M. A. *Chem. Phys. Lett.* **1981**, *83*, 362.

(10) The O–O bond distances in the transition state for oxygen atom transfer to ammonia were predicted to be 1.833 and 1.829 with CASSCF optimizations using (12e, 7 orb) and (12e, 9 orb).

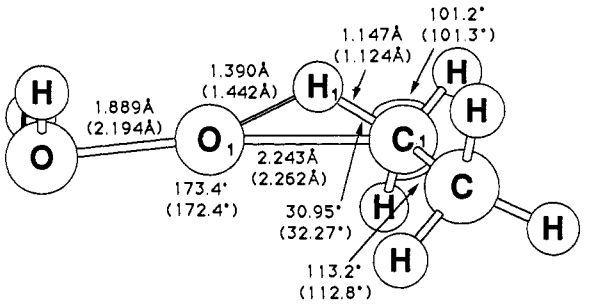

Figure 4. Transition structure for oxygen atom transfer from water oxide to ethane (**TS-2**) at the QCISD/6-31G* level, with corresponding CASSCF values in parentheses.

In order to assess the extent of electron transfer in the transition states, the natural orbitals for the UHF wave functions were obtained. For both methane and ethane transition structures (MP2/6-31G* geometries), all occupied orbitals except the HOMO had occupancies greater than 1.99, while the HOMO showed an occupancy of 1.74, and the LUMO showed an occupancy of 0.26. This suggested that there might be a significant level of electron transfer between these orbitals. However, given that the UHF wave functions were significantly spin-contaminated ($\langle S^2 \rangle \approx 0.45$), we checked this contention by performing a CASSCF calculation in the space of HOMO + LUMO.[9] At convergence, the occupation numbers of the CASSCF orbitals both for **TS-1** and **TS-2** were 1.96 and 0.04. A CASSCF calculation[6d] on **TS-2** with a larger active space was performed including the eight highest occupied orbitals from an RHF calculation and the three lowest virtual MOs (16 electrons in 11 orbitals). This more extensive calculation showed very little change in the occupation of the LUMO (0.05) but did indicate that there was 0.01 electron in each of the other two virtual orbitals. Thus the extent of electron transfer in a basis of correlated orbitals with the correct spin symmetry is relatively small, suggesting that the MP2 level provides an adequate description of the transition state.

To further investigate the question of open-shell character in the transition state, additional CASSCF calculations were performed on **TS-2**. To begin, the QCISD/6-31G* geometry was used to generate a set of UHF natural orbitals.[11] The UHF calculation showed significant spin-contamination ($\langle S^2 \rangle = 0.628$) and an orbital occupation of 1.619 for the HOMO and 0.381 for the LUMO, with all other orbitals being doubly occupied or empty. The UHF natural orbitals were used to start a CASSCF calculation with the valence space consisting of two electrons distributed in the HOMO and LUMO. Optimization of the geometry at the CASSCF level showed a significant increase in the O–O bond in **TS-2**. The CASSCF natural orbital occupancies were found to be at 1.975 and 0.025 for the HOMO and the LUMO, respectively. However, the UHF natural orbitals at the CASSCF geometry show occupancies of 1.390 and 0.610. Past experience has shown that the UHF method exaggerates the occupation of virtual orbitals, which may be attributed to the very large spin-contamination from other states ($\langle S^2 \rangle = 0.858$). The CASSCF calculation, on the other hand, imposes the correct spin symmetry and removes the spurious open-shell character predicted by the UHF method. Indeed, given the values of $\langle S^2 \rangle$ for these structures, the UHF description must be viewed with skepticism.

Inspection of the CASSCF orbitals show them to be bonding and antibonding combinations of the O–H–C fragment in **TS-2**. There is also a very small component of the O–O bond. To obtain suitable orbitals to describe the reactants, the transition-state CASSCF orbitals were used to start a calculation on water oxide and ethane with an interfragment distance of 100 Å. The optimization yields orbitals which are now essentially the bonding and antibonding O–O orbitals of water oxide with occupancies of 1.953 and 0.047, respectively. Given a correct zeroth-order description of the reactants and transition state, multireference CI calculations were performed on the basis of the CASSCF configurations.

The CASSCF calculation yields a **TS-2** barrier of 19.8 kcal/mol. Performing a multireference CI using the CASSCF orbitals and the two CASSCF configurations produces a modest lowering to give a barrier of 17.9 and 16.5 kcal/mol when the multireference Davidson correction is added. This differs markedly from the QCISD(T)//QCISD barrier of 7.4 kcal/mol. The difference is clearly attributable to the very much increased O–O bond length (0.3 Å) produced by the CASSCF optimization, which destabilizes the transition structure. In the MRCI calculations the values for the coefficient of the reference configuration (C_0) for both the transition state and the reactants were 0.93. This is almost identical to the C_0 obtained from a single reference CI calculation on the basis of SCF orbitals. There is little gained by the CASSCF method here. The dramatic shortening of the O–O bond appears to be brought about by the very much higher correlation effects in the QCISD wave function. It is, in principle, possible to perform a very much larger CASSCF calculation, but this makes the following MRCI impractical. In a related transition state involving oxygen donation, the O–O bond distance at the CASSCF level was not very sensitive to the size of the active space.[10] Given the profound effect of *dynamical* correlation on these transition structures,[5] it is inappropriate to simply perform excessive CASSCF calculations which are intended to deal with *nondynamical* correlation. From this study, we may conclude that the single reference QCISD(T)//QCISD approach is preferable (more tractable) to the MRCI//CASSCF approach, inasmuch as the geometry of the transition state must be obtained with a high-order wave function, to which some additional dynamical correlation must be added to obtain the correct energies.

(c) Oxygen Insertion into the Higher Alkanes. A frontier MO model of this type can be considered to be useful only if it can be related to experimental data and allow one to make meaningful mechanistic predictions about the pathway for oxygen atom insertion. Substituted dioxiranes have recently been shown to be powerful oxidizing agents that will attack saturated hydrocarbons in a highly regioselective manner. Electrophilic attack on long-chain aliphatic hydrocarbons occurs mainly at C_2 and C_3 to afford secondary alcohols as the kinetic product. Further oxidation to the corresponding ketone is typically observed. For example, oxidation of *n*-decane by dimethyldioxirane affords essentially 2- and 3-decanone with the former in larger amounts.[3c] Hence, the rate of oxygen insertion into the C–H bond of a secondary alcohol to afford the corresponding ketone is faster than oxidation of its saturated hydrocarbon precursor.[3f]

The overall mechanism described in eq 1 suggests that a lone pair of electrons on an adjacent oxygen should be more efficient in stabilizing the developing positive charge at carbon than a hydrocarbon fragment orbital on the alkyl group. To test this hypothesis we have examined several geometric orientations for the oxidation of methanol to acetaldehyde by the action of water oxide (Figure 5). The transition structure for oxygen insertion into methanol (**TS-3**) closely resembles **TS-2**, and the barrier is 4.7 kcal/mol lower than that for ethane. The faster rate of oxidation provides an explanation for ketone formation as the thermodynamic product in accord with experiment.[3a] In a manner analogous to that for ethane, the π_{CH_2} approach affords a first-order transition state, while the π_{CHOH} (**13**) and σ_{CH_2} (**14**) approaches afford second-order saddle points as established by frequency calculations at the MP2/6-31G* level (Figure 5).

(11) Hamilton, T. P.; Pulay, P. *J. Chem. Phys.* **1988**, *88*, 4926.

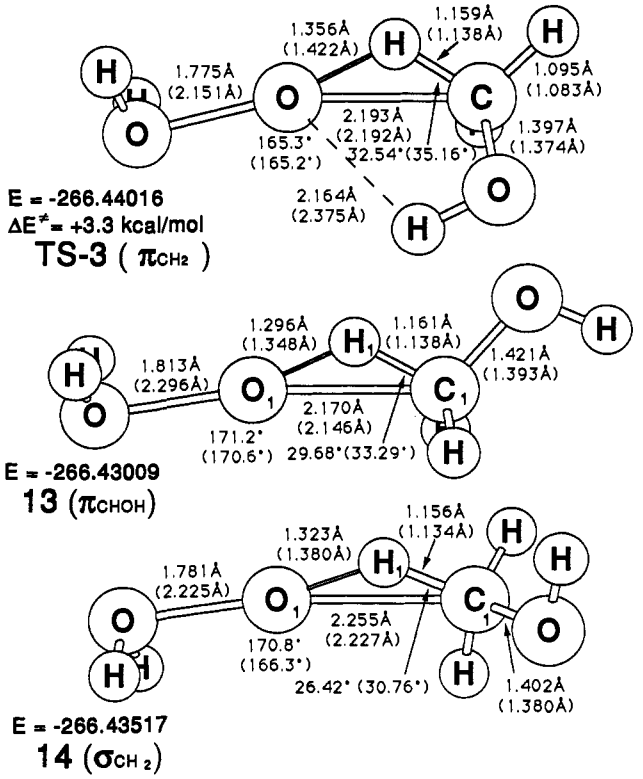

Figure 5. Transition structure **TS-3** and second-order saddle points **13** and **14** on the potential energy surface for oxygen atom transfer from water oxide to methanol. Geometries are MP2/6-31G* (HF/6-31G* values are in parentheses). Distances are in angstroms and angles in degrees. Energies are MP4SDTQ/6-31G*//MP2/6-31G*, au.

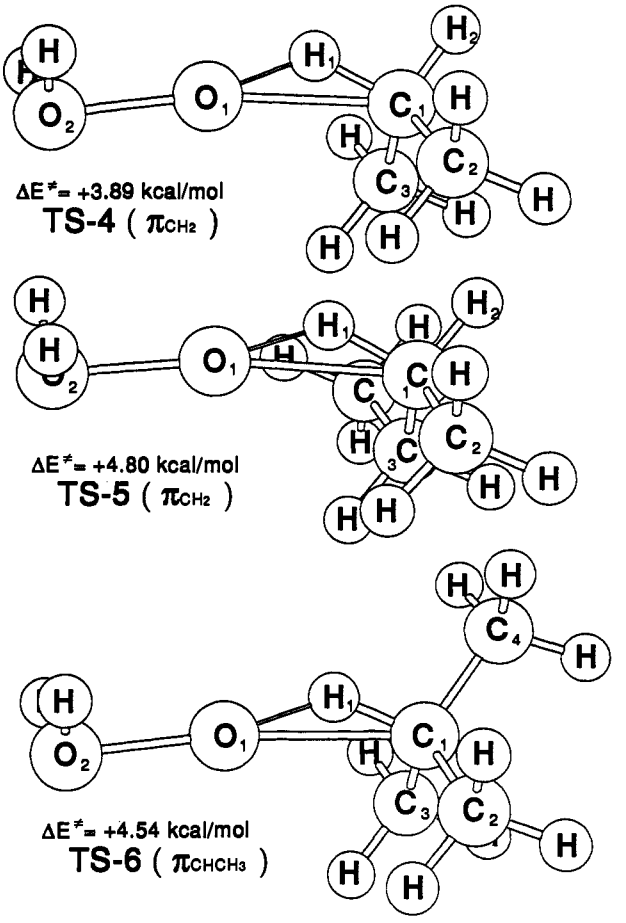

Figure 6. Transition structures for oxygen atom transfer from water oxide to propane (**TS-4**), butane (**TS-5**), and isobutane (**TS-6**) at the MP2/6-31G* level of theory. Activation barriers $\Delta E^{\ddagger}$ are MP4SDTQ/6-31G*//MP2/6-31G*.

Second-order saddle point **13** descends on the potential energy surface to **TS-3** by rotating the OH group. This rotation may be achieved by a positive as well as a negative rotation, hence there are two directions of descent from **13** to **TS-3**.

Although a cursory examination might suggest that all of the secondary carbon atoms of *n*-decane may be electronically similar, inspection of generalized transition state **5** clearly points out a serious steric problem. For example, oxygen insertion into *n*-decane at C_5 (R_1 = *n*-butyl, R_2 = *n*-pentyl) would afford a transition state that is much more sterically encumbered than one with $R_1 = CH_3$ and R_2 = *n*-octyl. Identification of the preferred π_{CH_2} or π_{CHR} fragment (eq 1) can, in principle, provide a reaction trajectory for approach of the electrophile and an explanation for this observed regiochemistry. To test this hypothesis we have examined the transition structures for the oxidations of propane and butane (Figure 6). At a lower level of theory we obtained a meaningful decrease in activation energy for oxygen atom insertion as the degree of alkyl substitution increased. Calculations at the HF/3-21G level suggested that barriers for oxygen insertion from water oxide into methane, ethane, propane (C_2), and *n*-butane (C_2) are 19.7, 16.8, 14.9, and 13.9 kcal/mol, respectively. However, at a level of theory that includes electron correlation (MP4SDTQ/6-31G*//MP2/6-31G*), we see a larger decrease for the second alkyl group, and these activation barriers are 10.7, 8.2, 3.9, and 4.8 kcal/mol, respectively. These data support the above explanation for the observed regiochemistry for oxidation of *n*-decane. The basic tenets of the FMO model approach depicted in **5** allow us to predict that an increase in the number of electron-donating alkyl substituents will stabilize the transition state for 1,2-hydrogen transfer to the approaching electrophile oxygen atom. While the energy differences for the various orientations of ethane oxidation are relatively small (Table I), increased complexity in the substrate, both sterically and electronically, will result in greater $\Delta\Delta E^{\ddagger}$. Referring to model transition structure **5**, we see the origin of a slight increase in activation energy ($\Delta\Delta E^{\ddagger}$ = 0.9 kcal/mol) for oxidation of a secondary carbon atom. In the oxidation of butane (**TS-5**, $R_1 = CH_3$, $R_2 = C_2H_5$) there is more steric congestion relative to oxygen insertion into propane (**TS-4**), where two methyl groups are at right angles to the trajectory of the incoming oxygen atom. The data in Table II show that the $H_1C_1H_2$ bond angle in **TS-4** and **TS-5** contract by ~6°, while the angle defining the steric interaction of the two alkyl groups ($C_2C_1C_3$) slightly expands (2–3.5°) relative to the geometry of the reactant alkane.

Electrophilic attack at a tertiary tetrahedral carbon may have three potential π_{CHR} transition states, *all of which would afford insertion with retention of configuration.* In **7**, R_3 is in the same plane as the migrating hydrogen, and inversion of configuration by interchanging R_3 with either R_1 or R_2 will produce two additional geometric orientations for approach of an electrophile. Similarly, there are three σ_{CHR} approaches that must be considered. Significantly, the barrier for oxygen atom insertion into isobutane relative to butane has slightly decreased to 4.5 kcal/mol. This reactivity trend suggests that both steric and electronic effects must play a role in the exclusive attack at a more highly substituted tertiary carbon. The C_1–O_1 bond distance increases from 2.280 in **TS-5** to 2.325 in **TS-6** as the nucleophilic carbon atoms become more sterically hindered. Although this should result in a slight increase in the activation barrier, the electronic influence of the additional alkyl group lowers the barrier.

With these data in hand we can identify the principal axis of reaction for an oxygen insertion reaction, and from an examination of molecular models we can suggest which tertiary carbon should be most accessible to electrophilic attack. High tertiary versus secondary selectivity has been observed in numerous examples of

Table II. Optimized Transition Structures for Oxygen Atom Transfer from Water Oxide to Propane, Butane, and Isobutane[a]

	H_2OO	propane	TS-4	butane	TS-5	isobutane	TS-6
$r(O_1O_2)$ (Å)	1.517 Å		1.774		1.772		1.762
$r(O_1H_1)$ (Å)			1.337		1.338		1.336
$r(H_1C_1)$ (Å)		1.096	1.152	1.097	1.154	1.098	1.151
$r(O_1C_1)$ (Å)			2.271		2.280		2.325
$r(C_1C_2)$ (Å)		1.526	1.514	1.525	1.515	1.526	1.516
$r(C_1C_3)$ (Å)		1.526	1.514	1.525	1.515	1.526	1.526
$r(C_1C_4)$ (Å)						1.526	1.524
$\angle H_1C_1O_1$ (deg)			26.14		25.72		22.38
$\angle C_2C_1C_3$ (deg)		110.9	114.4	112.9	114.9	110.8	112.6
$\angle H_1C_1H_2$ (deg)		106.1	100.2	106.2	100.2		
$\angle H_1C_1C_4$ (deg)						108.1	103.5
$\angle O_2O_1C_1$ (deg)			171.8		171.4		173.1
E_{MP4} (kcal/mol)	−151.071 56	−118.710 95	−269.776 32	−157.895 42	−308.959 33	−157.897 84	−308.962 17
$\Delta E^{\ddagger}$ [b] (kcal/mol)			3.89		4.80		4.54

[a] Geometries are at MP2/6-31G* and energies and barriers are at MP4SDTQ/6-31G*//MP2/6-31G*. [b] The zero-point energies are not included.

hydrocarbon oxidation with dioxiranes. Oxygen transfer from dimethyldioxirane to the stereoisomeric 1,2-dimethylcyclohexanes is a stereospecific insertion reaction affording a single tertiary alcohol in each case as the insertion product.[3c,d] The relative rate of oxidation of *cis*- and *trans*-1,2-dimethylcyclohexane is about 7:1 with methyl(trifluoromethyl)dioxirane (Mello dioxirane), but both reactions are stereospecific.[3d] Inspection of **15a** suggests that a π_{CHCH_3} approach across the top of the six-membered ring would be sterically hindered by the axial hydrogens, and the methyl group will hinder a σ_{CHCH_3} approach, as depicted in **15a**. The

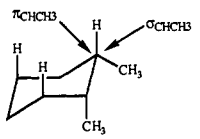

15a

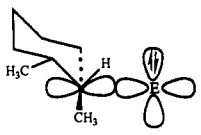

15b

π_{CHR} approach along the axis of the p orbital, as shown in **15b**, is the least hindered pathway, and we suggest that the TS for oxidation of *cis*-1,2-dimethylcyclohexane should resemble **15b**. Oxidation of the *trans* isomer of **15b** would be hindered by an axial methyl group at C_2.

One of the most striking examples of regioselective oxyfunctionalization is the direct hydroxylation at the side chain (C_{25}) of 5α-cholestan-3-one (**16**) in greater than 80% yield with either dimethyldioxirane or Mello dioxirane.[12]

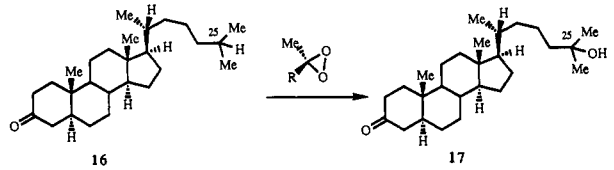

16 17

We suggest that the above C_{25} selectivity observed with **16** can be rationalized by considering the generalized mechanism outlined in eq 1. The only tertiary reaction site in **16** that can accommodate a gem dimethyl center is that at C_{25}. For the π_{CHR} orientation of attack in transition state **5**, the least hindered TS is one with $R_1 = R_2 = CH_3$. All other possible tertiary centers present some additional steric impedance to the approach of the dioxirane. In support of this suggestion, the σ_{CHCH_3} approach to isobutane in **18** (Figure 7) is a second-order saddle point that lies 0.5 kcal/mol higher in energy than **TS-6**. When entropy considerations are included, the $\Delta G^{\ddagger}$ for **TS-6** is 1.5 kcal/mol lower than that for second-order saddle point **18** (MP2/3-21G frequency calculation). When the third methyl group in isobutane is replaced by a larger substituent (e.g. **16**), we then anticipate that a much larger

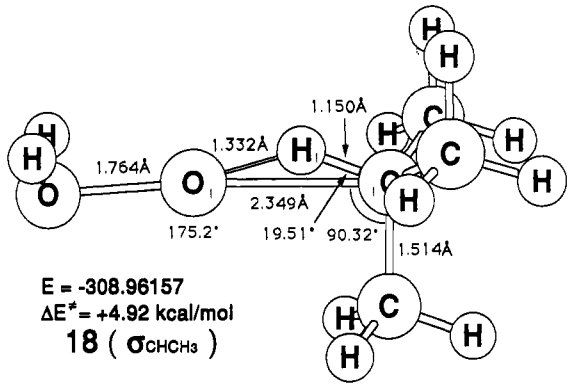

Figure 7. Second-order saddle points for oxygen atom transfer from water oxide to isobutane (**18**) at the MP2/6-31G* level of theory. Activation barriers are MP4SDTQ/6-31G*//MP2/6-31G*, au.

difference in energy between the various approaches would be observed. To generalize even further, we suggest that the lowest activation energy pathway for oxygen insertion into a tertiary center as depicted in **7** will have the two smaller substituents represented as R_1 and R_2, with the largest group, R_3, being in the plane of the migrating hydrogen (H_1). It is this juxtaposition of alkyl groups that provides the least steric hindrance and the lowest activation pathway for formation of the tertiary alcohol **17**. The steric requirements for these various oxidative processes obviously differ. However, in a qualitative sense, the principle orientation of attack of these novel reagents can be predicted using the basic concepts described in eq 1.

In summary, this FMO model provides an explanation for stereoselective oxygen insertion into a C–H bond at the most highly substituted carbon based upon electronic and steric considerations. The σ_{CH_2} approach for oxidation of methane appears to be anomalous since oxygen insertion into higher alkanes proceeds by interaction of a filled π_{CHR} orbital with the electrophilic oxygen. Identification of the proper π_{CH_2} or π_{CHR} fragment (eq 1) provides a reaction trajectory for the approach of the electrophile and an explanation for the retention of configuration. This theoretical analysis suggests that activation of an isolated σ(C–H) bond[1] is an oversimplification and that oxygen insertion involves perturbation of the entire π_{CHR} fragment orbital. This qualitative FMO analysis, supported by *ab initio* molecular orbital calculations, places emphasis upon the approach of an electrophile to a filled fragment orbital containing both a carbon 2p orbital and a hydrogen atom for the insertion of E into a σ C–H bond. The H_1–C–E bond angle in **5** varies from 22 to 32° depending upon the steric interactions involved. We emphasize that the approach of E sometimes deviates from the idealized σ and π trajectories described. A rotation about the C–E axis of 60° can interconnect σ and π approaches. The primary purposes of this model are to allow predictions of an

(12) Bovicelli, P.; Lupattelli, P.; Minicione, E.; Prencipe. T.: Curci, R. *J. Org. Chem.* **1992**, *57*, 5062.

approximate reaction pathway and to provide an explanation for the selectivity observed in hydrocarbon insertion reactions. This FMO model appears to be quite general, since insertions of carbenes into hydrocarbons are also consistent with eq 1, where the empty p orbital of the singlet carbene interacts with a filled σ_{CH_2} hydrocarbon fragment orbital and concomitant hydrogen migration to the adjacent carbene lone pair occurs.[13] Preliminary *ab initio* results also indicate that hydrocarbon insertion reactions of rhodium proceed by electrophilic attack of an electron-deficient orbital on a filled hydrocarbon fragment orbital. Finally, we feel that this FMO model will ultimately provide an overall unified mechanism for hydrocarbon insertion reactions.

(13) Singlet methylene insertion in this manner occurs without a barrier. For a higher energy TS with hydrogen migration to the opposite side of the carbene lone pair, see: Gordon, M. S.; Gano, D. R. *J. Am. Chem. Soc.* **1984**, *106*, 5421.

Acknowledgment. This work was supported in part by the National Institute of Health (CA 47348-03), the Ford Motor Company, a NATO Collaborative Research Grant (900707), and the C.I.R.I.T. of the "Generalitat de Catalunya." We are also thankful to the Pittsburgh Supercomputing Center, CRAY Research, the Ford Motor Company, the computing center at Wayne State University, the University of Manchester regional computing center, and SERC (U.K.) for generous amounts of computer time.